

Supporting Information

Achieving ultra-high anisotropy in thermal conductivity of plastic crystal through megapascal pressure of hot pressing

Zhipeng Wu^{1, #}, Mingzhi Fan^{2, #}, Yangjun Qin^{1,3, #}, Guangzu Zhang^{2, †}, Nuo Yang^{3, †}

1) School of Energy and Power Engineering, Huazhong University of Science and Technology, Wuhan 430074, China

2) School of Intergrated Circuits, Huazhong University of Science and Technology, Wuhan 430074, China

3) Department of Physics, National University of Defense Technology, Changsha 410073, China

Z. W., M. F. and Y. Q. contributed equally to this work.

†Corresponding E-mail: G.Z. (zhanggz@hust.edu.cn) and N.Y. (nuo@nudt.edu.cn)

SM I. Details of sample preparation

Preparation of $[(\text{CH}_3)_4\text{N}][\text{FeCl}_4]$ involves the following steps. 1.6218 g of iron(III) chloride hexahydrate (AR, Aladdin) is accurately weighed and dissolved in 4 mL hydrochloric acid (AR, Sinopharm), resulting in solution A after 30 minutes of stirring. Simultaneously, an equimolar amount (0.6756 g) of tetramethylammonium chloride (>98%, Aladdin) is dissolved in deionized water (4 mL), leading to solution B after 30 minutes of stirring. The two solutions, A and B, are then mixed and stirred thoroughly to obtain a clear and transparent yellow solution. At 70°C, a rapid solution evaporation process was employed for 5 hours to obtain powder samples for powder X-ray diffraction (XRD) testing. If the solution is allowed to stand for approximately 10 days, yellow crystals will precipitate from the solution, which is $[(\text{CH}_3)_4\text{N}][\text{FeCl}_4]$.

Then, plastic crystal films were fabricated. 5 mg plastic crystal was heated to 150 °C and maintained at the temperature for 10 minutes. Subsequently, a pressure (4 MPa, 6 MPa, 7 MPa, 8 MPa, or 16 MPa) was applied and maintained for 20 minutes. After the pressure was released, a dense $[(\text{CH}_3)_4\text{N}][\text{FeCl}_4]$ film was formed. Then the films were employed for thermal conductivity testing, differential scanning calorimetry (DSC), XRD, scanning electron microscopy (SEM), and infrared temperature testing. The basic information of the films is provided in Table S1.

The phase structures of the powders and films were analyzed using X-ray diffraction (XRD; 7000 S/L, Shimadzu Corp., Japan). Differential scanning calorimetry (DSC; Perkin Elmer Instruments, USA) was performed to determine the phase transition temperatures and heat capacity over a temperature range of 275-425 K, with

a heating rate of 5 K min⁻¹ in a nitrogen atmosphere. Scanning electron microscopy (SEM; Nova NanoSEM 450, Netherlands) was employed to observe the surface and cross-sectional morphology of the films. The temperature distribution of thin films can be measured by infrared temperature testing (FOTRIC, China).

Table S1: The basic information of the [(CH₃)₄N][FeCl₄] films

Pressure(MPa)	Thicknesses(μm)	Density(g/cm ³)
4	96	1.55
6	84	1.56
7	70	1.57
8	69	1.58
16	52	1.61

SM II. Details of measurements.

This study employed the 3-Omega method to measure the thermal conductivity of organic plastic crystal film [(CH₃)₄N][FeCl₄]. The traditional uniaxial heat conduction model of 3-Omega requires direct deposition of metal electrodes on the surface of the test film. However, due to the flexibility of organic films, depositing nano-electrodes on their surface can cause electrode deformation or even fracture. Therefore, for organic films, a bidirectional asymmetric heat conduction model is typically used, and the formula is shown as Equation S1[1, 2]. In this model, metal electrodes are first deposited on the substrate surface, and then the test film is bonded to the electrodes to protect the metal electrodes. For anisotropic films, the frequency-temperature rise

signal from a single metal electrode cannot provide the thermal conductivity in both the in-plane and cross-plane directions. This is because when the electrode width is much larger than the film thickness, the electrode is only sensitive to the cross-plane thermal conductivity. However, when the electrode width is comparable to or smaller than the film thickness, the electrode becomes sensitive to both in-plane and cross-plane thermal conductivities. Therefore, by using two metal electrodes with different widths, the in-plane and cross-plane thermal conductivities of the test film can be obtained[3].

The thickness of the plastic crystal films prepared in this experiment ranges from 40 to 100 μm . Considering the accuracy of signal measurements, the width of the metal electrodes in the 3-Omega method should not be too large. Therefore, the width of the metal electrodes in this experiment is all below 200 μm . Consequently, the electrodes are sensitive to the thermal conductivity in both directions [4]. First, the experiment needs to select a certain frequency interval to ensure that the thermal penetration depth can penetrate the film to be measured, and then measure the $V_{3\text{-}\omega}$ signal at different frequencies, as shown in Figure S1.

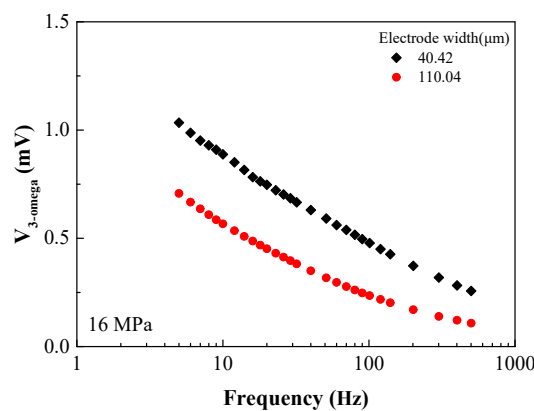


Figure S1: $V_{3\text{-}\omega}$ in relation to frequency

After obtaining the relationship between $V_{3\text{-}\omega}$ and frequency, the thermal conductivity is obtained by fitting the theoretical temperature rise with the experimental temperature rise using the least squares method. For a single electrode, both the thermal conductivity in the cross-plane direction and the anisotropy ratio are unknowns. According to Equation S1, by providing a series of anisotropy ratios (η), the corresponding thermal conductivity in the cross-plane direction (κ_{cross}) can be obtained. Then, by using the experimental signals from two electrodes of different widths, a set of relationships between κ_{cross} and η can be obtained. Since the κ_{cross} and η of the test film are constant, the intersection point of the curves represents the true κ_{cross} and η of the film.

$$\Delta T = \frac{P}{2\pi l} \int_0^{\infty} \frac{1}{\gamma_j} \frac{(A^+ + A^-)(B^+ + B^-) \sin^2(\lambda b)}{A^+ B^- - A^- B^+} \frac{d\lambda}{(\lambda b)^2} \quad (S1)$$

$$\gamma_j = \kappa_{cross, i} \sqrt{\eta_i \lambda^2 + \frac{2i\omega}{\alpha_{cross, i}}} \quad (S2)$$

Here, P , l and b represent the heating power, length, and half-width of the metal electrode, respectively; A^+ , A^- , B^+ and B^- are dimensionless parameters obtained by solving equations using the recursive matrix method; λ is the integration variable; $\kappa_{cross, i}$ and $\alpha_{cross, i}$ are the thermal conductivity and thermal diffusivity in the cross-plane direction of the i th layer, respectively.

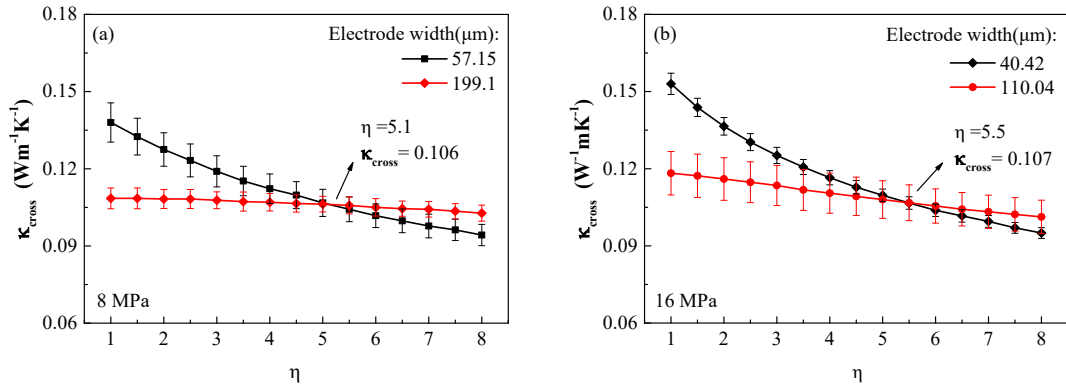


Figure S2: Thermal conductivity fitting results of the plastic crystal film: (a) 8 MPa; (b)16 MPa.

SM III. Details of the EMD simulation.

In this work, the equilibrium method of molecular dynamics (EMD) was used to calculate the thermal conductivity, and all the simulation details are given in Table S1. The Green-Kubo formula is a result of linear response theory and the fluctuation dissipation theorem, which relates the heat flow autocorrelation to the thermal conductivity. k_B is the Boltzmann constant, V is the volume of the system, T is the temperature, τ is the relaxation time, τ_0 is the heat flux upper limit of the autocorrelation function, E is the kinetic energy of all atoms in the system, N is the number of atoms, and angular bracket is the system average. All molecular dynamics simulations in this paper are performed using the LAMMPS software package. The interatomic forces are taken from the universal force field [5] and the bond angles are taken from consistent valence force field [6]. The relevant parameters are listed in Table S2. This represents a challenging aspect of the simulation because the force fields are not specially developed for $[(CH_3)_4N][FeCl_4]$. In the simulations, the structure cannot keep a perfect crystal structure of $[(CH_3)_4N][FeCl_4]$, which takes error in the calculations. It may

minimize the error by specially developing a force field for $[(\text{CH}_3)_4\text{N}][\text{FeCl}_4]$ [7].

The long-range Coulombic force is calculated using the particle-particle particle-mesh (PPPM) method with an error parameter of 10^{-5} . Periodic boundary conditions are applied in all three dimensions. And the velocity verlet algorithm is employed to integrate equations of motion. 0.25 fs and 10 Å are chosen as time step and cutoff distance for the Lennard-Jones interaction, respectively. In addition, 8 independent simulations with different initial conditions are conducted to get better average. The simulation structures are simulated in NPT ensembles at target temperatures and 0 atm for 125 ps to obtain the optimized structures and simulation cell sizes, then followed by NVT ensembles for 125 ps before collecting heat flux of all six directions in NVE ensembles for 4 ns.

Table S1: Details of the simulation parameters.

Method		EMD (Green-Kubo method)			
Force field		Universal force field Consistent valence force field			
Boundary conditions		x y z: p p p			
Simulation process					
Ensemble	Setting				Purpose
NPT	Time step(fs)	0.25	Runtime(ns)	0.5	Relax structure
	Temperature(K)	330	Pressure(atm)	0	
NVT	Time step(fs)	0.25	Runtime(ns)	0.5	

	Temperature(K)	330	Thermostat	Nose- Hoover	
NVE	Sample interval time (fs)	3	Runtime(ns)	4	Data process
	Correlation time (ps)	25	Temperature(K)	330	
Recorded physical quantity					
Temperature			$\langle E \rangle = \sum_{i=1}^N \frac{1}{2} m_i v_i^2 = \frac{3}{2} N k_B T$		
Heat flux			$J = \frac{1}{V} \left[\sum_i e_i \vec{v}_i + \frac{1}{2} \sum_i \vec{r}_{ij} (\vec{F}_{ij} \cdot \vec{v}_i) \right]$		
Thermal conductivity			$\kappa = \frac{V}{3k_B T^2} \int_{\tau}^{\tau_0} \langle \vec{J}(0) \cdot \vec{J}(\tau) \rangle d\tau$		

Table S2: Parameter of force field

Atom type	Charge(e)	ϵ (kcal/mol)	σ (Å)
C	0.2481	0.105	3.851
Fe	3	0.013	2.912
Cl	-1	0.227	3.95
N	-0.6284	0.069	3.66
H	0.053	0.044	2.886

SM IV. Details of the relationship between thermal conductivity and the (002) crystal plane.

To investigate the relationship between the (002) crystal plane and thermal conductivity, it is calculated that the ratio (R_{XRD}) between this the integrated intensities of planes parallel to (002) and the sum of integrated intensities related to the other planes. The values of R_{XRD} and the ratio of thermal conductivity (R_{κ}) between the value along in-plane direction and cross-plane direction are plotted in Figure S3. It can be observed that the trend of R_{XRD} and R_{κ} with the pressure are similar, supporting that the preferential orientation of crystals influences thermal conductivity.

Compared to films prepared at 8 MPa, there is a slight decrease in (002) peak intensity and obvious decrease in (102) in the 16 MPa sample. Moreover, the XRD pattern for the 16 MPa film shows only three distinct peaks, indicating a closer resemblance to a single-crystal state. This could due to the formation of nearly single-crystal structure under higher pressure, which is shown in cross-sectional SEM images.

Combined with MD simulation results, it is evident that perfect plastically crystalline structures exhibit higher thermal conductivity along the (002) and (020) plane. Therefore, despite the slight decrease in (002) peak intensity for films prepared at 16 MPa, the formation of a more prominent, nearly single-crystal structure enhances their in-plane thermal conductivity.

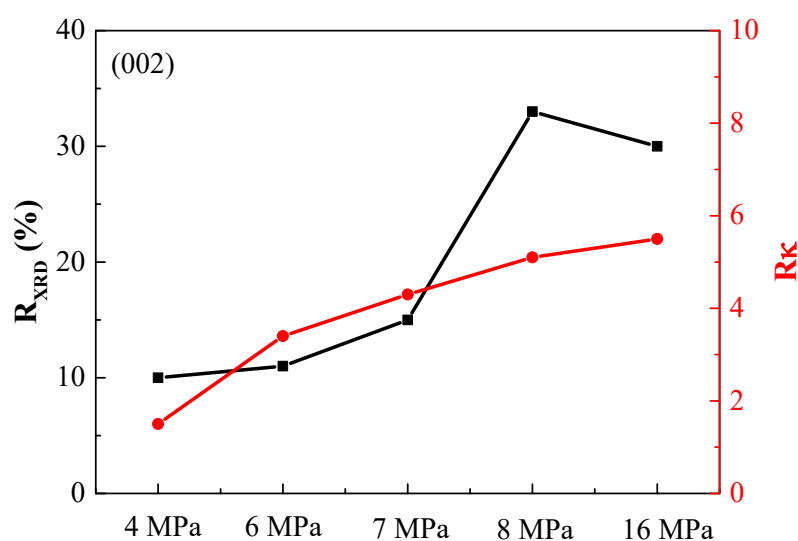


Figure S3. The values of R_{XRD} of (002) and R_k of films under different pressure.

SM V. Analysis of the Effects of Density and Porosity on the Thermal Conductivity of Plastic Crystals

As for the impact of density, quantitative measurements reveal that the density of the PCs film is changed 4% within the pressure range from 4 to 16 MPa, as shown in Table S1. This can be attributed to the inherent plasticity of $[(\text{CH}_3)_4\text{N}][\text{FeCl}_4]$, which, under uniaxial pressure, causes the crystal to elongate along other directions, resulting in small changes in density. Therefore, density has minimal impact on the thermal conductivity of the PCs film in this study.

Furthermore, the change of porosity is also not large because it is related to the density. There are many grain boundaries in porous structures, which cannot introduce anisotropy in thermal conductivity. As the increase of pressing, the porous structures and the number of boundaries is diminishing and the increasing crystal structures take

the anisotropy. Then, the phonon mean free path of crystal structures should be much larger than that of porous structures.

The anisotropic thermal conductivity of the PCs material studied here is primarily influenced by the microstructure and orientation of crystal structures.

From the SEM cross-sectional image (Figure 4) and XRD data (Figure 2(d)), it is evident that the film pressed at 4 MPa exhibits an unordered polycrystalline structure with disordered porous crystals. As the pressure increases, large layered grains gradually form within the film, and the intensity of the (002) crystal plane peak increases. Under 8 MPa hot-pressing, a clear formation of large layered grains is observed in the upper half of film samples.

Under 16 MPa hot-pressing, larger and more distinct single-crystal-like structures emerge within the film, forming pronounced layered structures, as shown in Figure 4(d) of the main text. Its XRD pattern shows only three main peaks: (002), (111), and (020), with other peaks either disappearing or weakening, also indicating that the film approaches a single-crystal state.

Additionally, MD simulation results (Figure 5) show that a perfect single-crystal structure exhibits significant thermal conductivity anisotropy, with the highest thermal conductivity along the [100] and [010] directions (parallel to the (002) crystal plane). Therefore, as the pressure increases, the crystals preferentially orient along the (002) plane, forming more complete layered structures that approach a single-crystal state, leading to an increase in the in-plane thermal conductivity and a significant thermal conductivity anisotropy in the film.

References

- [1] Feldman, A., High Temp-High Press 1999(31): p. 293.
- [2] Tong, T. and A. Majumdar, *Reexamining the 3-omega technique for thin film thermal characterization*. Review of Scientific Instruments, 2006. **77**(10).
- [3] Borca-Tasciuc, T., A.R. Kumar, and G. Chen, *Data reduction in 3 ω method for thin-film thermal conductivity determination*. Review of Scientific Instruments, 2001. **72**(4): p. 2139-2147.
- [4] Yamaguchi, S., T. Shiga, S. Ishioka, et al., *Anisotropic thermal conductivity measurement of organic thin film with bidirectional 3 ω method*. Review of Scientific Instruments, 2021. **92**(3).
- [5] Rappe, A.K., C.J. Casewit, K.S. Colwell, et al., *UFF, a full periodic table force field for molecular mechanics and molecular dynamics simulations*. Journal of the American Chemical Society, 1992. **114**(25): p. 10024-10035.
- [6] Dauber-Osguthorpe, P., Roberts V.A., Osguthorpe D.J., et al., *Structure and energetics of ligand binding to proteins: Escherichia coli dihydrofolate reductase-trimethoprim, a drug-receptor system*. Proteins: Structure, Function, and Bioinformatics, 1988. **4**(1): p. 31-47.
- [7] Qin Y., Zong Z., Che J., Li T., Fang H., Yang N., *Unveiling the thermal transport mechanism in compressed plastic crystals assisted by deep potential*. . arXiv:2501.12078, 2025.